Li *et al. Microstructures* 2023;3:2023024
DOI: 10.20517/microstructures.2023.09

Microstructures

Review

Open Access

Check for updates

Recent developments in metal nanocluster-based catalysts for improving photocatalytic CO_2 reduction performance

Huan Li[1], Huitong Du[2], Huanhuan Luo[2], Hua Wang[3], Wenlei Zhu[2], Yang Zhou[1]

[1]Key Laboratory of Organic Electronics and Information Displays, Institute of Advanced Materials (IAM), Nanjing University of Posts & Telecommunications, Nanjing 210023, Jiangsu, China.
[2]State Key Laboratory of Analytical Chemistry for Life Science, State Key Laboratory of Pollution Control and Resource Reuse, Frontiers Science Center for Critical Earth Material Cycling, School of Chemistry and Chemical Engineering, School of the Environment, Nanjing University, Nanjing 210023, Jiangsu, China.
[3]Huzhou Key Laboratory of Medical and Environmental Applications Technologies, School of Life Sciences, Huzhou University, Huzhou 313000, Zhejiang, China.

Correspondence to: Prof. Wenlei Zhu, State Key Laboratory of Analytical Chemistry for Life Science, State Key Laboratory of Pollution Control and Resource Reuse, Frontiers Science Center for Critical Earth Material Cycling, School of Chemistry and Chemical Engineering, School of the Environment, Nanjing University, Nanjing 210023, Jiangsu, China. E-mail: wenleizhu@nju.edu.cn; Prof. Yang Zhou, Key Laboratory of Organic Electronics and Information Displays, Institute of Advanced Materials (IAM), Nanjing University of Posts & Telecommunications, Nanjing 210023, Jiangsu, China. E-mail: iamyangzhou@njupt.edu.cn

How to cite this article: Li H, Du H, Luo H, Wang H, Zhu W, Zhou Y. Recent developments in metal nanocluster-based catalysts for improving photocatalytic CO_2 reduction performance. *Microstructures* 2023;3:2023024. https://dx.doi.org/10.20517/microstructures.2023.09

Received: 3 Feb 2023 **First Decision:** 16 Mar 2023 **Revised:** 26 Apr 2023 **Accepted:** 8 May 2023 **Published:** 22 May 2023

Academic Editor: Chunqiang Zhuang **Copy Editor:** Fangling Lan **Production Editor:** Fangling Lan

Abstract

Photocatalytic reduction of carbon dioxide (CO_2) is a promising technology for carbon recycling that offers both environmental and economic benefits. Among the potential photocatalysts, metal nanoclusters (MNCs) stand out as a class of materials with remarkable photophysical and photochemical properties. Despite the growing number of studies on MNCs-based photocatalytic reduction of CO_2 in recent years, a systematic and comparative overview of these studies is still lacking. This review provides a concise and comprehensive summary of the latest research on MNCs-based catalysts for enhancing photocatalytic CO_2 reduction performance. Moreover, this review highlights the challenges and opportunities in this field based on the current development trends.

Keywords: Photocatalysis, CO_2 reduction, nanoclusters, photocatalyst

INTRODUCTION

Fossil fuels have been the dominant source of energy for various applications such as production, transportation, and power generation throughout human history. However, the excessive consumption of fossil fuels has led to the massive emission of carbon dioxide (CO_2), which poses serious threats to energy security and environmental quality[1-9]. Numerous carbon fixation strategies have been developed to address these challenges, such as CO_2 emission reduction, CO_2 capture and storage (CCS), and CO_2 utilization[10-12]. CO_2 emission reduction involves the use of innovative technologies to lower the amount of CO_2 produced during the production stage. However, these methods are often associated with high costs that are difficult for the general public to bear. The CCS also received significant attention, but the high cost and leakage risk limit its application on a large scale. CO_2 utilization, in contrast, is the most attractive path. Chemical reforming, electrochemical reduction, biological reduction, and photochemical reduction are the leading CO_2 utilization technologies. Photocatalytic CO_2 reduction (PCR) is a sustainable process. It does not produce any toxic byproducts or cause any environmental pollution. PCR process can harness solar energy to reduce CO_2 and produce valuable energy sources such as methane or methanol. Moreover, the PCR process is usually operating under mild conditions of ambient temperature and pressure. These advantages make PCR a highly desirable method for completing the carbon cycle[13-20].

In the past few decades, the development of PCR catalysts has shifted from early bulky metals to nanostructured materials with specific properties[21]. Nanoclusters (NCs) are a new class of materials comprising a few to several hundred atoms surrounded by ligands. NCs have three components: the inner core, the outer atoms, and the surface ligands (as shown in Figure 1)[22]. NCs exhibit distinct physical and chemical properties compared to nanoparticles and molecules due to their distinctive electronic and geometric structures. The majority of the current NCs are metal nanoclusters (MNCs) with sizes ranging from 0.1 to 5 nm (typically < 2 nm for MNCs)[23], which is close to the Fermi wavelength (approximately 0.7 nm). Due to the quantum size effect, a single atomic change can drastically alter the electronic structure and the physical and chemical properties of the clusters. Compared to conventional nanoparticles, MNCs possess a much higher proportion of surface atoms. The surface atoms of MNCs have a low coordination number, which results in high activity[24]. Furthermore, MNCs are easier to synthesize than individual atoms and also have a larger surface area and more catalytic sites than bulk materials[25].

Taking advantage of these inherent advantages, MNCs have been used as catalysts in various catalytic processes. For example, Kurashige *et al.* investigated Au NCs as co-catalysts for H_2 evolution[26]. Gautam *et al.* presented a series of Au_n(GSH) NCs as co-catalysts on $BaLa_4TiO_{15}$ for photocatalytic water splitting[27]. Numerous efforts also have been devoted to the development of MNCs-based photocatalysts to further improve PCR performance[28]. For instance, Shoji *et al.* reported Cu_xO NCs as a general co-catalyst and can be used in combination with various semiconductors to construct low-cost and efficient PCR systems[29]. Similarly, Gao *et al.* also reported Ag NCs as co-catalysts for selective CO_2 photoreduction to CO[30]. Additionally, Bo *et al.* bridged Au NCs with ultrathin nanosheets via ligands for enhancing charge transfer in PCR[31]. All these relevant reports above confirm that MNCs are promising catalyst candidates for PCR.

However, the synthesis and utilization of MNCs for PCR remain challenging. It requires a comprehensive understanding of their properties and catalytic reaction mechanisms. In this review, we provide a systematic overview of the recent advances in MNCs-based catalysts for PCR applications. We first introduce a general

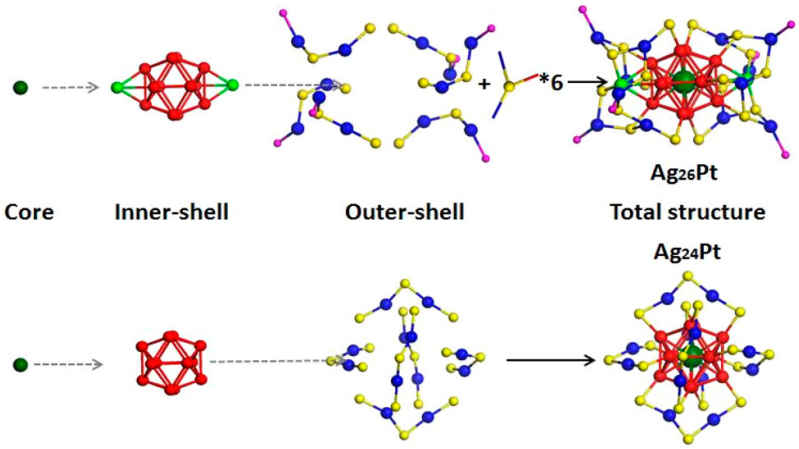

Figure 1. Structures of MNCs of $Ag_{26}Pt$ and $Ag_{24}Pt$[22]. Copyright 2018, American Chemical Society.

method for preparing MNCs. Next, we review how MNCs can enhance the PCR process as catalysts. We then classify the MNCs into two major categories: noble and nonnoble MNCs and summarize their advantages for PCR applications. Finally, we discuss the current challenges and prospects of MNCs for PCR. We hope this review will stimulate further research and innovation in this emerging field.

ADVANTAGES OF MNCS AND COMMON SYNTHESIS METHODS

Advantages of MNCs

MNCs show a very different energy level structure in comparison with large-size nanoparticles (as shown in Figure 2). MNCs change the electron energy level near the Fermi level from quasi-continuous to discrete, resulting in energy level splitting or energy gap widening[32,33]. The discrete energy levels allow the electrons in MNCs to jump between energy levels and interact with light, which enhances the separation of electrons and holes[34]. Additionally, MNCs also have a small energy gap and absorb light in the visible and near-infrared regions[35,36]. Furthermore, MNCs are stable against oxidation or reduction by photogenerated electrons or holes[37,38]. More importantly, MNCs have a high specific surface area, a high fraction of low-coordinated atoms, a quantum size effect, a tunable composition, and a unique surface structure (e.g., pocket-like sites) due to their ultra-small size. These unique features of MNCs make them an emerging class of photocatalytic materials with increasing interest[39]. Moreover, their precise atomic-level structures enable fundamental research on the photocatalytic mechanisms, which provides theoretical guidance for the design of new photocatalytic materials and improves catalytic performance[40].

The synthesis methods of MNCs

There has been much research into the synthesis of MNCs, so we have summarized the commonly reported synthesis methods in the literature as follows[41]:

(1) Reduction growth method[42] (as shown in Figure 3 a→c): The metal core is created by reducing the respective metal ions. Therefore, the strength of the chosen reducing agent and the kinetic regulation of the reduction process are crucial for synthesizing the desired product.

(2) Seed growth method[43] (as shown in Figure 3 c→d): Smaller-sized MNCs are used as seeds to induce nucleation, resulting in the growth of larger-sized MNCs over time. The regulation of the crystal growth process is noteworthy.

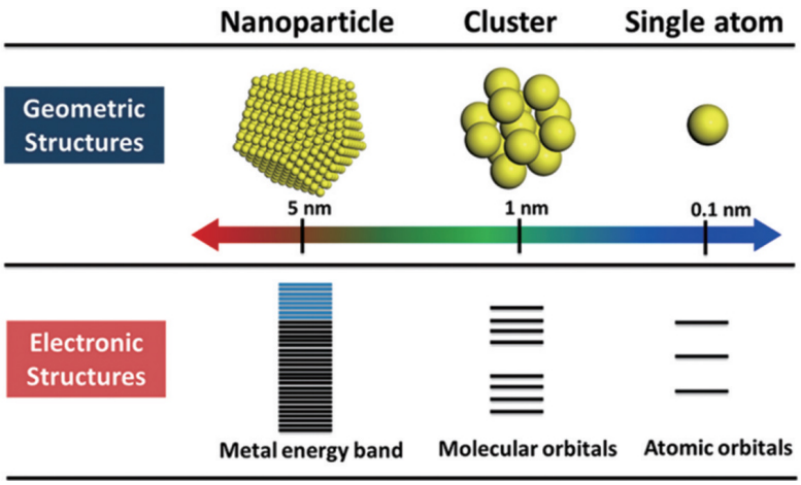

Figure 2. Geometric and electronic structures of single atoms, NCs, and nanoparticles[23]. Copyright 2018 American Chemical Society.

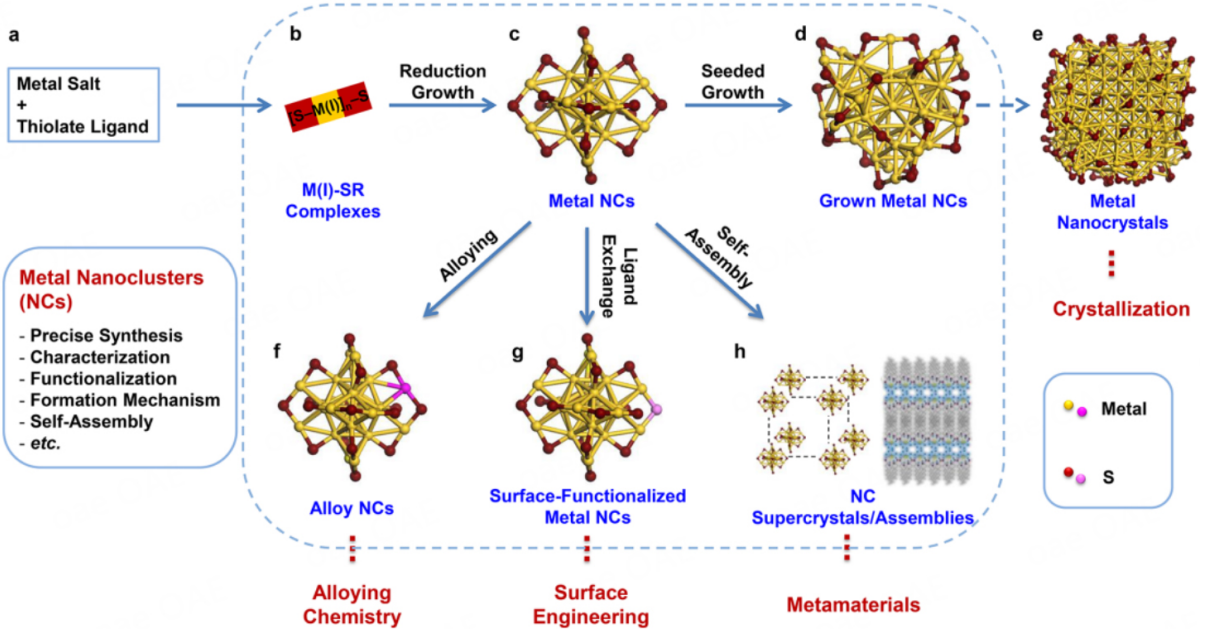

Figure 3. Common methods for the synthesis of MNCs: (a→b) formation of M(I)-SR complexes, metal atom (M(I)), thiolate ligand (SR), (b→c) reduction growth, (c→d) seeded growth, (c→f) alloying reaction, (c→g) ligand-exchange process, (c→h) self-assembly of metal NCs, and (d→e) evolution from metal NCs to metal nanocrystals[41]. Copyright 2016, American Chemical Society.

(3) Alloying method[44] (as shown in Figure 3 c→f): The introduction of other metals for doping could be accomplished through the template exchange method, where the difference in electrode potential between the two metals serves as the driving force for the substitution reaction.

(4) Ligand exchange method (as shown in Figure 3 c→g): In principle, the ligand exchange method is similar to the alloying method in that both involve an exchange process, but the objects exchanged differ. For example, template exchange generates alloying NCs, whereas ligand exchange refers to preparing MNCs by exchanging the protective ligand layers on their periphery.

(5) The current atomically precise nano-chemistry is indeed moving toward the programmable synthesis of MNCs with control over the structure, such as the bcc, fcc, hcp, decahedra, icosahedra, multi-tetrahedral network, *etc.* (as shown in Figure 4)[45,46]. This programmable synthesis of MNCs offers promising opportunities for designing their structures and enhancing their catalytic performance[47].

THE PCR MECHANISM OVER MNCS-BASED PHOTOCATALYSTS

PCR involves multielectron reduction, and various products can be obtained via different reduction pathways, such as CO, CH_4, HCOOH, C_2H_4, HCHO, and CH_3OH. Below are the reduction potentials (E_0, V *vs.* NHE) required for these products:[48]

$$CO_2 + e^- \rightarrow CO_2^- \; E_0 = -1.900 \text{ V} \quad (1)$$

$$CO_2 + 2H^+ + 2e^- \rightarrow HCOOH \; E_0 = -0.610 \text{ V} \quad (2)$$

$$CO_2 + 2H^+ + 2e^- \rightarrow CO + H_2O \; E_0 = -0.530 \text{ V} \quad (3)$$

$$2CO_2 + 2H^+ + 2e^- \rightarrow H_2C_2O_4 \; E_0 = -0.913 \text{ V} \quad (4)$$

$$CO_2 + 4H^+ + 4e^- \rightarrow HCHO + H_2O \; E_0 = -0.480 \text{ V} \quad (5)$$

$$CO_2 + 6H^+ + 6e^- \rightarrow CH_3OH + H_2O \; E_0 = -0.380 \text{ V} \quad (6)$$

$$CO_2 + 8H^+ + 8e^- \rightarrow CH_4 + 2H_2O \; E_0 = -0.240 \text{ V} \quad (7)$$

$$2CO_2 + 12H^+ + 12e^- \rightarrow C_2H_4 + 4H_2O \; E_0 = -0.349 \text{ V} \quad (8)$$

$$2CO_2 + 14H^+ + 14e^- \rightarrow C_2H_6 + 4H_2O \; E_0 = -0.270 \text{ V} \quad (9)$$

$$3CO_2 + 18H^+ + 18e^- \rightarrow C_3H_7OH + 5H_2O \; E_0 = -0.310 \text{ V} \quad (10)$$

The ultra-small size of NCs gives them a strong quantum size effect, exhibiting discrete energy levels that allow electrons to undergo a leap from the highest occupied molecular orbital (HOMO) to the lowest unoccupied molecular orbital (LUMO), and electron-hole separation occurs. The energy gap of MNCs is typically less than 2.2 eV, allowing photocatalytic reactions under visible light irradiation. Therefore, MNCs can be considered semiconductor nanomaterials for photocatalytic reactions with small band gaps.

The mechanism of MNCs as catalysts in the PCR process is as follows (as shown in Figure 5)[49,50]. After irradiating the MNCs-based catalyst with light with photon energy equal to or greater than the band gap energy, the electrons transfer from the valence band (VB) to the conduction band (CB) to generate photogenerated electrons and holes. The photogenerated holes are transferred to the surface active sites for the oxidation reaction, as shown in process (1) of Figure 5[51]. In process (3) of Figure 5, photogenerated electrons are transferred to the surface-active site for the reduction reaction. Therefore, the photocatalytic performance is affected by the incident light absorption capacity and charge separation efficiency. To fully utilize the energy from solar radiation, the band gap of the photocatalyst should be below 3.1 eV to maximize light absorption[52]. Most of the solar radiation energy reaching Earth is in the visible spectrum. Additionally, the generated electrons and holes do not always migrate to the surface of the photocatalyst

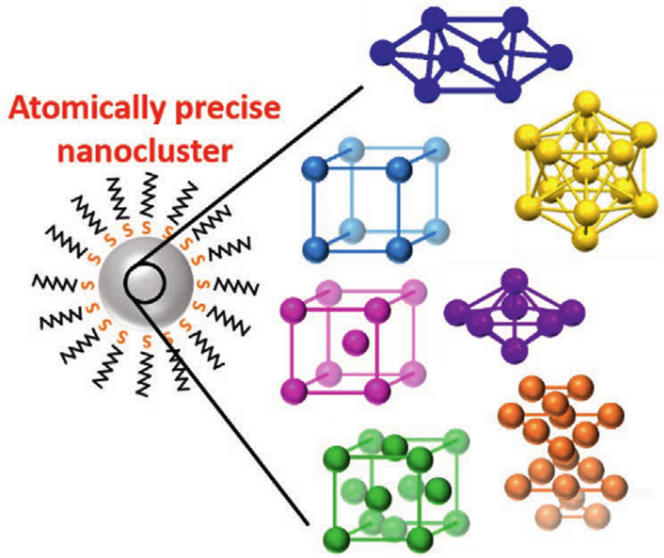

Figure 4. Programmable atomic packing into different crystal structures of Au NCs[45]. Copyright 2021, Wiley-VCH.

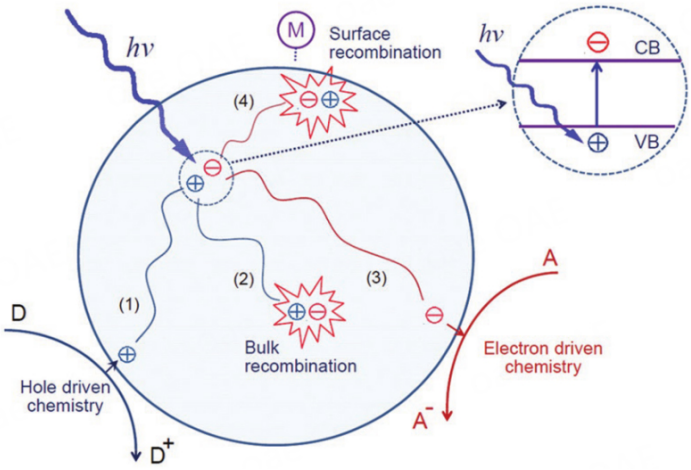

Figure 5. Photocatalytic process of MNCs[49]. Copyright 1995, American Chemical Society.

and react optimally. Occasionally, photogenerated electrons and holes will combine inside the catalyst [as shown in process (2) in Figure 5] or on the surface [as shown in process (4) in Figure 5] in a brief period, releasing energy in the form of heat or light that can result in a significant reduction in photocatalytic efficiency.

Therefore, the MNCs-based materials used to improve the PCR process must satisfy the following conditions: (1) Smaller energy gaps, typically exhibiting significant absorption in the visible or near-infrared region, make it easier to form photogenerated electron-hole pairs; (2) Good photostability, not readily oxidized or reduced by photogenerated holes or electrons. Long lifetimes of photogenerated electrons and holes so that the electron-hole pairs can participate more in redox reduction; and (3) The large specific surface area provides more catalytic sites, allowing free electrons to react with CO_2 via charge transfer to the composite surface[53].

PROGRESS OF MNCS-BASED CATALYSTS IN PCR

MNCs have garnered attention for their potential to improve PCR performance due to their unique and desirable properties. Several reasons contribute to the focus on MNCs for PCR, including:

(1) High catalytic activity: The small size and high surface area-to-volume ratio of MNCs result in a high catalytic activity, which can enhance the efficiency of the PCR.

(2) Improved charge transfer: MNCs have been shown to improve the charge separation and transfer processes in photocatalytic systems, leading to higher photocatalytic activity.

(3) Tailor-made properties: The properties of MNCs can be easily tuned or customized by controlling the size, shape, and composition, allowing for better control of their catalytic activity.

Overall, MNCs have shown great potential for enhancing PCR performance. Continued research on MNCs can contribute to the development of sustainable and efficient CO_2 reduction systems. Many strategies have been proposed to use MNCs as catalysts for improving PCR performance. This section reviews the recent advances in MNCs-based catalysts for enhancing PCR performance. We classify the MNCs-based catalysts into two subsections, nonnoble (e.g., Cu[54], CdS[55], Fe, Co[56], Ni, Cu) and noble MNCs-based (e.g., Au[57], Ag[58], Pt) catalysts[59]. Then, we describe their respective roles as catalysts for improving the PCR process. The photocatalytic performance of various MNCs-based catalysts under visible-light irradiation is presented in Table 1.

Nonnoble MNCs-based catalysts in PCR

Nonnoble MNCs offer a wide range of material selection options, and commonly available and inexpensive metals such as Fe, Ni, Cu, and Al can be used to prepare MNCs. Additionally, they are generally less costly compared to noble MNCs, resulting in lower preparation costs. In addition, semiconductor materials with wide energy gaps, such as TiO_2, $SrTiO_3$, $BiVO_4$, Ta_3N_5, g-C_3N_4, CdS, and MoS_2, are the most widely used photocatalysts[60]. However, most required light sources are in the ultraviolet spectrum, with low solar utilization and high electron-hole complexation rates, resulting in low photocatalytic reaction efficiency[61-63]. Consequently, using nonnoble MNCs as co-catalysts is suitable for overcoming these disadvantages[64]. Due to the advantages mentioned above, nonnoble MNCs-based catalysts are primarily employed for surface modification of semiconductor materials to enhance PCR performance. The reaction process for nonnoble MNCs-based catalysts to improve PCR performance by surface modification techniques has two steps, namely visible-light-induced interfacial charge transfer (IFCT) between the MNCs and semiconductor materials and the multielectron reduction of oxygen molecules mediated by the co-catalytic promoter effect of the MNCs[65].

Preparation of nonnoble MNCs-based catalysts by impregnation to enhance PCR performance

Photocatalysts composed of nonnoble MNCs and semiconducting materials are typically fabricated by the impregnation method[66]. Impregnation is a method of incorporating one material into another by soaking or spraying the material onto the surface of the other. Impregnation involves the following steps: The prepared semiconducting material is soaked or sprayed with the MNCs' solvent, which contains a suspension of MNCs, and allowed to dry. The MNCs are then deposited onto the surface of the semiconducting material. The impregnated semiconducting material is then calcined at high temperatures to remove the solvent and stabilize the MNCs on the surface of the semiconducting material. The impregnation method allows for the controlled deposition of MNCs onto the surface of semiconducting materials, thereby preparing materials with good photocatalytic activity.

Table 1. Performance of various noble & nonnoble MNCs used for PCR

Sample	Performance	References
Cu (II)-TiO_2	CO_2 generation rate = 0.13 μmol/h; quantum efficiency = 27.7%	[67]
Cu(II)-Nb-doped TiO_2	CO_2 generation rate = 0.20 μmol/h; quantum efficiency = 25.3%	[69]
Cu(II)-TiO_2 after the coordination of oxygen and metal	CO_2 generation rate = 0.40 μmol/h; quantum efficiency = 68.7%	[75]
Fe(III)-TiO_2	CO_2 generation rate = 0.40 μmol/h; quantum efficiency = 53.5%	[77]
Fe(III)-Ti(IV)-TiO_2	CO_2 generation rate = 0.69 μmol/h; quantum efficiency = 92.2%	[79]
Ni/TiO_2	CH_3CHO production rate = 1.42 μmol g-cat^{-1}	[81]
TiO_{2-x}/CoO_x	CO production rate = 1.2473 μmol/g/h; CH_4 production rate = 0.0903 μmol/g/h	[82]
CeO_x-S/$ZnIn_2S_4$	CO productivity of 1.8 mmol/g$^{/}$ with a rate of 0.18 mmol/g/h	[83]
Au NCs/TiO_2/Ti_3C_2 with CBD method	CO yield of 27.5 μmol/g in 3 h; CH_4 yield of 42.11 μmol/g in 3 h	[87]
SNO/CdSe–DET	CO production rate = 36.16 μmol/g/h	[102]
Au-NC@UiO-68-NHC	CO production rate = 57.57 μmol/g/h	[107]

The initial focus of the research was to improve the visible light sensitivity of TiO_2 semiconductors by using Cu(II) or Fe(III) NCs as co-catalysts (as shown in Figure 6)[67,68]. However, this photocatalytic system has limited catalytic efficiency because IFCT occurs only at the TiO_2/MNCs interface. Liu *et al.* designed a TiO_2 photocatalyst that can respond to visible light based on the principle of energy level matching[69]. The energy level occupied by the N-doped particles below the conduction band of TiO_2 matches the potential of the Cu^{2+}/Cu^{+} redox couple in the Cu(II) NCs. The matched energy levels facilitate the efficient transfer of photogenerated electrons from the doped Nb state to the Cu(II) NCs, thereby contributing to the efficient multielectron reduction of oxygen molecules (as shown in Figure 7)[69,70]. This method provides a practical and strategic approach to creating new MNCs materials with effective photocatalytic properties.

Nonnoble MNCs-based catalysts improve PCR performance by increasing vacancies and defects

Nonnoble MNCs-based catalysts are not limited to simple grafting modifications as co-catalysts. It was discovered that the performance of PCR could be enhanced by increasing the vacancies and defects. By generating oxygen vacancies, these modifications increase the surface negative charge density[71]. Upon exposure to light, the oxygen vacancies accumulate additional negative charges that contribute to the extension of the visible light absorption of semiconductor material, making the metal oxide capable of activating CO_2[72].

Nolan *et al.* present a study of electron and hole localization in low-coordinated titanium and oxygen sites of free and metal oxide-supported TiO_2 nanocrystals (as shown in Figure 8A)[73]. This approach highlights how nonnoble MNCs can enhance oxygen and metal coordination by modifying semiconductor materials. The structure of MNCs as catalysts in semiconductors reveals a significantly different metal and oxygen coordination environment compared to that of the unmodified semiconductor[74,75]. Low-coordinated metal and oxygen sites are crucial as charge carrier capture sites and active sites for target molecules, such as carbon dioxide and water[76]. Thus, Liu *et al.* developed a more sophisticated synthesis strategy by employing MNCs with poorly coordinated metal and oxygen sites as catalysts[77,78]. Liu *et al.* also demonstrated that amorphous Ti(IV) NCs promoted the oxidation of organic compounds effectively (as shown in Figure 8B) and that TiO_2 with Fe(III) and Ti(IV) NCs as catalysts achieved a Q.E. of 90% (as shown in Figure 8C)[79]. Additionally, Cheng *et al.* recently published the first study on Cu clusters mediated into Cd vacancies at the edges of CdS nanorods for photocatalytic CO_2 conversion[80]. Billo *et al.* reported a Ni-NCs/TiO_2 catalyst with improved PCR performance[81]. The Ni-NCs and O vacancies provide energetically stable CO_2 binding sites for CO_2 reduction, allowing for rapid electron transport for enhanced solar energy harvesting[81]. This method enhances the photocatalytic activity and selectivity of Ni/TiO_2 via a synergistic interaction in which

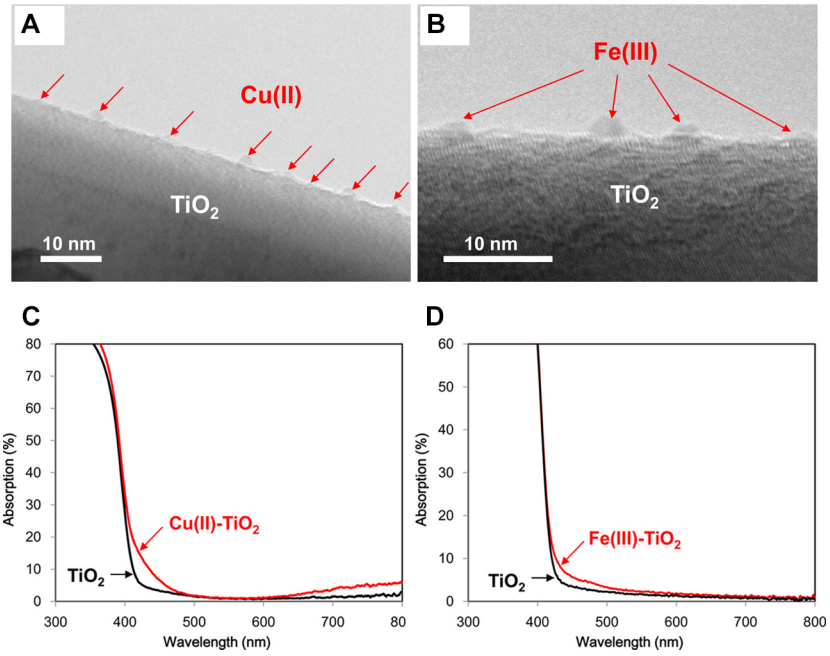

Figure 6. Cu (II) (A) and Fe (III) (B) NCs-grafted TiO_2 images captured by TEM. UV-Vis absorption spectra for Cu(II) (C) and Fe(III) (D) NCs-grafted TiO_2[70]. Copyright 2016, American Chemical Society.

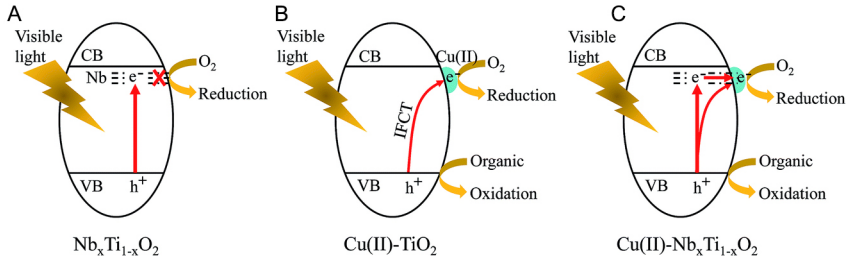

Figure 7. Proposed photocatalytic processes for (A) $Nb_xTi_{1-x}O_2$, (B) Cu(II)-TiO_2, and (C) Cu(II)-$Nb_xTi_{1-x}O_2$, respectively[70]. Copyright 2016, American Chemical Society.

the active center increases activity by lowering the activation barrier energy for CO_2 dissociation, and CO_2 molecules can bind to Ni and defect sites. Li *et al.* developed an effective photothermal catalyst by modifying TiO_2 nanotubes with a minute amount of CoO_x and oxygen vacancies. The results demonstrated that introducing oxygen vacancies facilitated the charge separation and dispersion of CoO_x co-catalysts, in which grafted CoO_x acted as hole traps and promoted the release of more protons (as shown in Figure 9)[82]. In addition, Hou *et al.* have significantly enhanced the activity by constructing CeO_x NCs with surface defect sites via a "partial sulfation" technique. The underlying principle of this strategy is improving the surface electronic properties of CeO_x-S NCs, which in turn induces the appearance of several Ce^{3+} and oxygen vacancies[83]. The photogenerated electrons were captured by oxygen vacancies on the CeO_x-S/$ZnIn_2S_4$ catalyst and subsequently transferred to CO_2, promoting CO_2 activation (as shown in Figure 10). This discovery also provides information regarding the optimization of PCR.

Noble MNCs-based catalysts in PCR

While the high cost of noble MNCs limits their use in large quantities, they possess large energy bandwidths and high electron densities that enable them to rapidly receive and release electrons. This results in the high

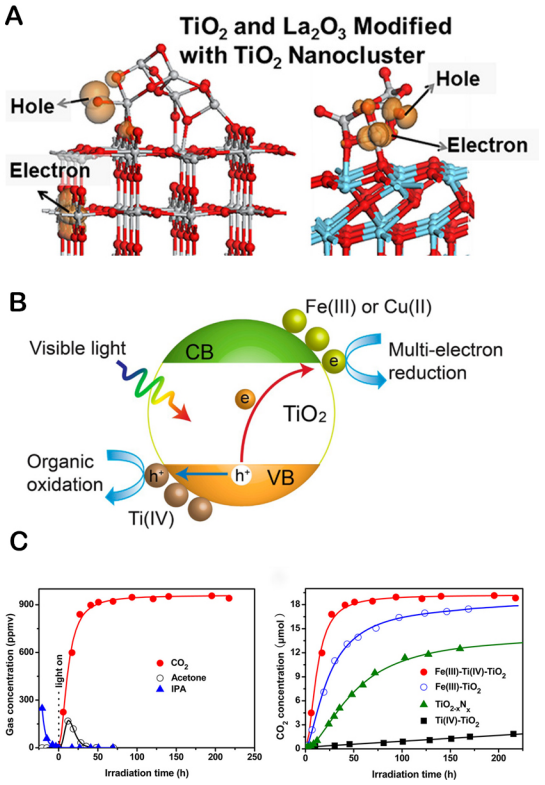

Figure 8. (A) Atomic structure of TiO_2 and La_2O_3 modified with TiO_2 NCs[73]. Copyright 2014, American Chemical Society. (B) Proposed photocatalysis processes. (C) Photocatalytic performance of the Fe(III)-Ti(IV)-TiO_2 nanocomposites[79]. Copyright 2014, American Chemical Society.

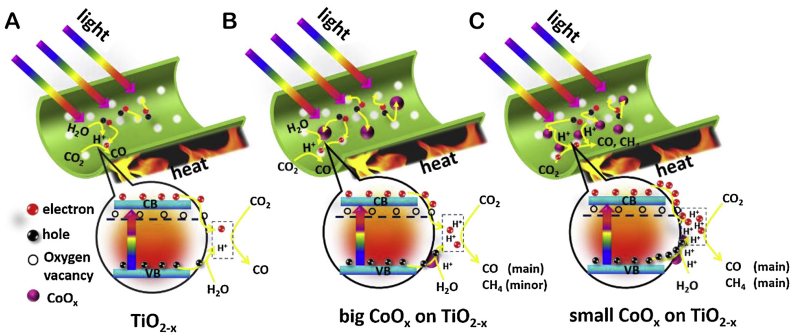

Figure 9. Scheme of photothermocatalytic reaction over three typical samples: (A) TiO_{2-x}. (B) big CoO_x clusters modified TiO_{2-x}. (C) small CoO_x clusters modified TiO_{2-x}[82]. Copyright 2018, Elsevier.

catalytic activity of noble MNCs[84]. Noble MNCs are also known to exhibit unique electrical and thermodynamic properties, which allow them to perform reactions that other catalysts cannot. For instance, they are being utilized in biological research.

Noble MNCs-based catalysts improve PCR performance by cluster beam deposition

The acids and ligands used in conventional surface modification techniques have a chemical contamination effect on the MNCs (the effect causes the change of a single atom to have a significant physical and chemical effect on the MNCs). Cluster beam deposition (CBD) was proposed to avoid the chemical contamination of

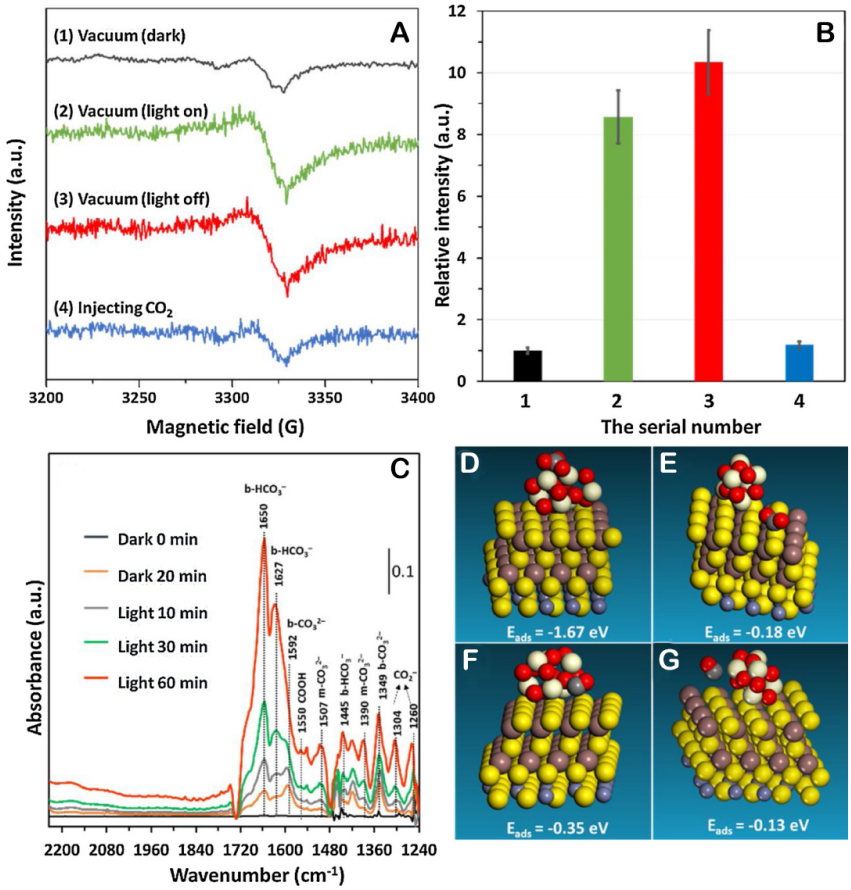

Figure 10. Investigation of the promotional role of CeO_x-S clusters in electron transfer and the subsequent surface reaction. (A) *In situ* EPR signals of CeO_x-S/$ZnIn_2S_4$. (B) Quantitative analysis by the double integral of the EPR signals in a. (C) *In situ* FTIR spectra for the adsorption, activation, and reduction of CO_2 under visible light over CeO_x-S/$ZnIn_2S_4$. (D and E) Adsorption energies of CO_2 and (F and G) CO at different sites of Ce_6O_{10}-$ZnIn_2S_4$ (0001) determined by DFT calculations[83]. Copyright 2018, Elsevier.

MNCs. CBD produces cluster-modified semiconductor materials with exceptional photocatalytic properties by forming clusters in a gaseous environment and then soft-landing them on supports with precise control over their size, shape, and composition (as shown in Figure 11)[85]. After deposition, unlike wet chemistry, no additional calcination or activation steps are required[86]. The vapor-phase Au NCs deposition method permits the placement of all active particles on the surface. Li *et al.* also prepared Au NCs/TiO_2/Ti_3C_2 and Au nanoparticles/TiO_2/Ti_3C_2 by deposition and precipitation[87]. The optimized Au NCs/TiO_2/Ti_3C_2 exhibited higher yields of reduced CO_2 to CO and CH_4 than Au-nanoparticles/TiO_2/$TiCO_2$ and P-Au-nanoparticles/TiO_2/$TiCO_2$ (as shown in Figure 12)[87]. CBD for MNCs synthesis not only reduces the risk of chemical contamination but also ensures that the MNCs are evenly distributed over the semiconductor surface and reduces costs.

Preparation of Noble MNCs-based catalysts by preventing clusters from aggregating improve PCR performance

Due to their large specific surface area and high surface energy, noble MNCs are typically thermodynamically unstable and susceptible to migration and agglomeration under light irradiation or high-temperature conditions, resulting in a substantial decrease in catalytic activity and selectivity[88,89]. Therefore, strategies to prevent cluster aggregation on the carrier are necessary to enhance their photocatalytic performance[90].

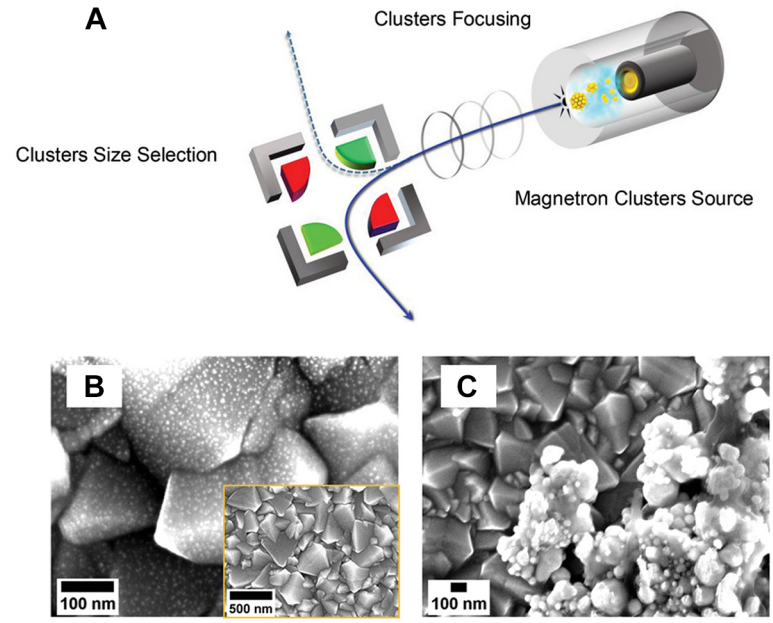

Figure 11. (A) Schematic illustration of magnetron CBD technology. High-Resolution SEM images of (B) Au NCs modified FTO and (C) colloidal Au modified FTO. The inset image in (B) shows the global view of deposited Au NCs[85]. Copyright 2021, Wiley-VCH.

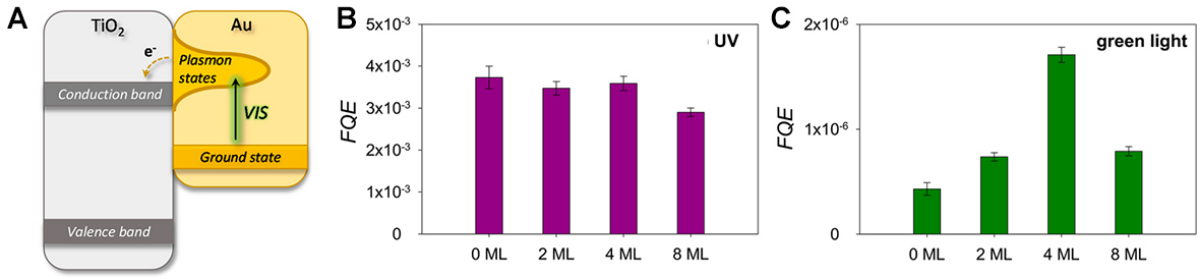

Figure 12. (A) Schematic illustration of hot electron transfer from an excited plasmonic state on the gold nanoparticle to the TiO_2 conduction band. Formal Quantum Efficiency (FQE) under (B) UV and (C) green light illumination as a function of Au NCs coverage on TiO_2 P25[86]. Copyright 2018, Wiley-VCH.

Bard proposed traditional Z-scheme photocatalysts in 1979[91], which can improve charge separation efficiency and retain strong redox capabilities. This system consists of two semiconducting materials with appropriate intermediate couples, such as Fe^{3+}/Fe^{2+}, IO^{3-}/I^-, and I^{3-}/I^-[92]. These two semiconductors have band structure configurations that differ. In a perfect process, photogenerated holes in the VB of PC I react with electron donors to produce electron acceptors. Photogenerated electrons in PC II's CB react with electron acceptors to produce electron donors. Then, photogenerated electrons in PC I's CB and holes in PC II's VB participate in the reduction and oxidation reactions, respectively (as shown in Figure 13)[93,94]. This mode of charge transfer can endow this system with powerful redox capability and spatially distinct redox reaction sites. Deng *et al.* developed PCR catalysts based on Z-scheme Au NCs (as shown in Figure 14)[95]. By combining with the photogenerated electrons in the coupled semiconductor, the photogenerated holes in the Au NCs can be consumed. This combination prevents the self-oxidative aggregation of Au NCs and increases their stability, thereby enhancing their photocatalytic activity[95]. Therefore, it is essential to combine NCs with suitable semiconductors when constructing a Z-scheme heterojunction system.

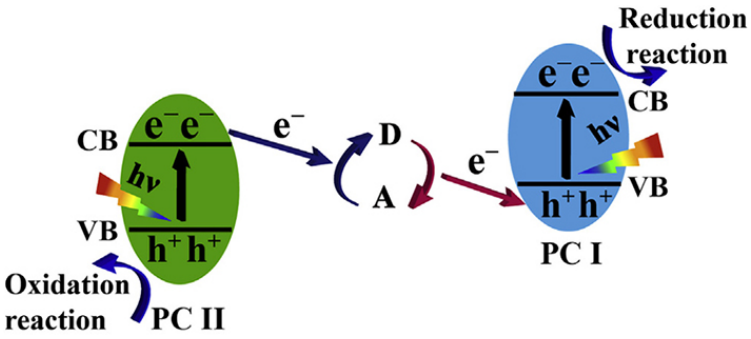

Figure 13. Schematic illustration of charge transfer in traditional Z-scheme heterojunction photocatalysts. D in the figure indicates electron donors, and A in the figure indicates electron acceptors[94]. Copyright 2020, Elsevier Inc.

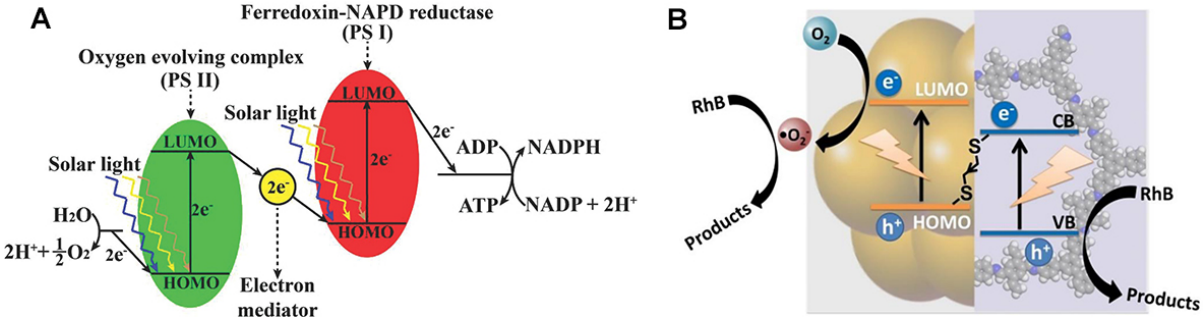

Figure 14. (A) A Z-scheme photocatalytic mechanism in natural photosynthesis system[90]. Copyright 2014, WILEY-VCH. (B) Photogenerated electron transport rules between Au NCs and COF support[95]. Copyright 2020, Wiley-VCH.

In addition to Z-scheme heterojunction structures, S-scheme heterojunctions are utilized to fabricate catalysts for improving PCR performance. (as shown in Figure 15A)[96]. S-scheme heterojunction has the following advantages: (1) the photocatalytic system can have both a wide photo-response range and a strong redox ability; (2) the large internal contact area and the rapid separation of carriers in the S-scheme system suppress the photo-induced electron-hole pair combination, which further improves the photocatalytic ability[97-101]. Ke *et al.* initially fabricated a novel S-scheme SNO/CdSe-DET composite and investigated its PCR activity (as shown in Figure 15B)[102]. The SNO/CdSe-DET composites exhibited excellent CO_2 photoreduction stability. Such a superior activity should be ascribed to the S-scheme system, which benefits the separation of the photogenerated carriers and promotes the synergy between CdSe-DET nanorods and SNO nanosheets by strong chemical-bonding coordination.

The encapsulation of MNCs in metal-organic frameworks (MOFs) has also garnered considerable interest[103,104]. By encapsulating MNCs within the environment of the MOFs structure, their fluctuations and aggregation can be effectively reduced, resulting in improved stability and catalytic efficiency. The MOFs structure prevents MNCs from interacting with undesirable species in the reaction environment, which can have a detrimental impact on their performance. Furthermore, the highly porous and interconnected structure of MOFs enables the efficient mass transfer of molecules to and from the active sites of MNCs, thereby enhancing their catalytic activity[105]. Overall, the MOFs-encapsulated MNCs show enhanced stability and improved performance, making them highly attractive for improving PCR performance. Indrani Choudhuri and Donald G. Truhlar studied a composite material containing a Cd_6Se_6 cluster in the pore of NU-1000 MOF. The Cd_6Se_6@NU-1000 composite permits electron transfer from the visible-light photo-excited organic linker to the lowest unoccupied orbital of the inorganic cluster, which can result in

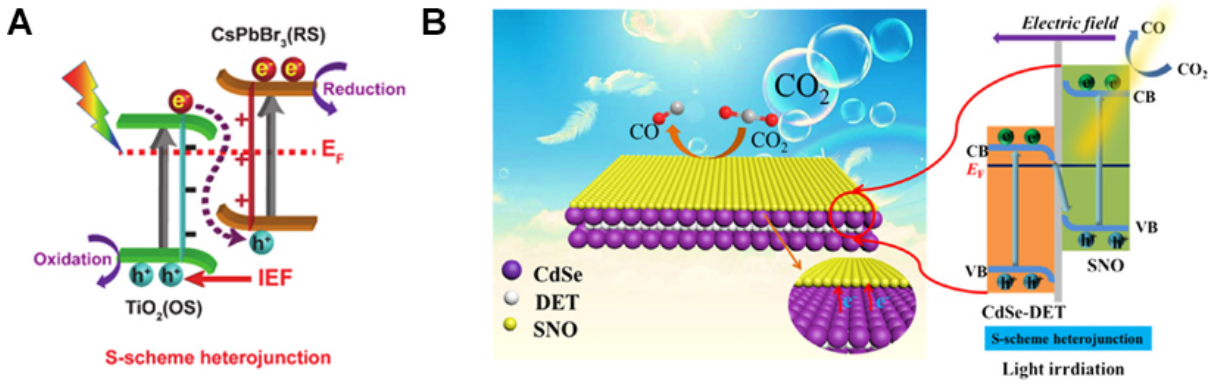

Figure 15. (A) S-scheme heterojunction. (B) The S-scheme SNO/CdSe-DET heterojunction charge migration and separation diagram under light irradiation[102]. Copyright 2021, Wiley-VCH.

charge separation (as shown in Figure 16A and B)[106]. Jiang *et al.* present a heterogeneous nucleation strategy for stabilizing and dispersing ultrasmall Au NCs in an NHC-functionalized porous matrix (as shown in Figure 16C)[107]. The Au NCs are embedded in the MOF material to prevent cluster aggregation. It gives the composite material a high degree of photostability and chemical stability. During the PCR process, the Au-NC@MOF composite demonstrates outstanding and consistent activity (as shown in Figure 16D)[107]. Therefore, MOFs are ideally suited for photocatalysis design.

Noble MNCs-based catalysts improve PCR performance by photosynthetic biohybrid system

Noble MNCs exhibit excellent biocompatibility, minimizing interference with the inherent functions of living organisms. This advantage allows noble MNCs to be used in the biological field. To link pre-assembled biosynthetic pathways with inorganic light absorbers, a photosynthetic biohybrid system (PBS) was developed. Both the high light-harvesting efficiency of solid-state semiconductors and the superior catalytic performance of whole-cell microorganisms are inherited by this strategy[108]. For instance, Zhang *et al.* utilized Au NCs as biocompatible intracellular light absorbers in PBS[109]. A biocompatible light absorber circumvents slow electron transfer kinetics and functions of the existing PBS as an inhibitor of reactive oxygen species to maintain high bacterial activity. With the dual advantages of light absorption and biocompatibility, this PBS can efficiently absorb sunlight and transfer photogenerated electrons to cellular metabolism, allowing for several days of continuous CO_2 fixation (as shown in Figure 17)[109]. The method of constructing PBSs offers a novel concept for PCR.

To summarize, compared to noble MNCs-based catalysts, nonnoble MNCs-based catalysts have a lower price, greater availability, a more comprehensive selection of materials, and better stability. The disadvantage is that the catalytic effect of the PCR process is inferior to that of noble MNCs. Furthermore, noble MNCs-based catalysts exhibit better biocompatibility. However, the scarcity of precious metals causes them to be expensive. The high specific surface area of noble MNCs-based catalysts can cause aggregation. Maintaining the long-term stability of the composites under *in situ* light conditions is challenging, a bottleneck in developing noble MNCs-based catalysts for practical applications. Thus, adopting strategies to prevent cluster aggregation on the carrier (such as Z/S-scheme heterojunction or MOF structure) is essential for their photocatalytic performance.

SUMMARY AND PROSPECTS

Artificial carbon fixation has stimulated the development of PCR as a promising technology. MNCs are a new potential photocatalyst with unique physical and chemical properties. To improve PCR performance,

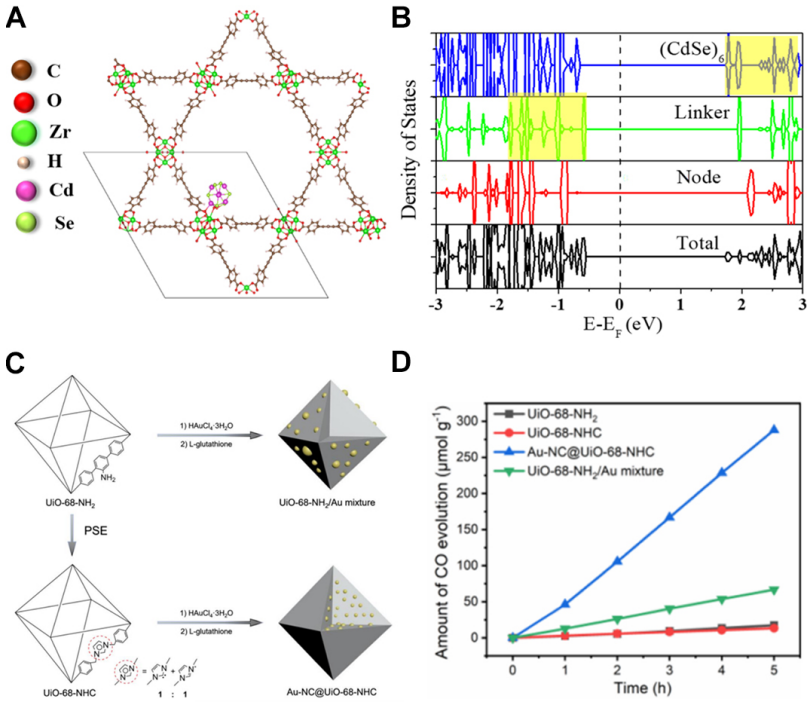

Figure 16. (A) Structure of the Cd_6Se_6 cluster encapsulated in NU-1000 at a node site (Cd_6Se_6@NU-1000). The unit cell of the system is denoted by a solid line. (B) Total and partial density of states of Cd_6Se_6@NU-1000. The Fermi level is set to zero and denoted by a black dashed line. The highest occupied crystal orbital (HOCO) is on the linker, and the lowest unoccupied crystal orbital (LUCO) is on the cluster. The highest-energy occupied orbitals on the linker and the lowest-energy unoccupied orbitals on the cluster are highlighted in yellow[106]. Copyright 2020, American Chemical Society (C) Schematic presentation for the synthesis of UiO-68-NHC, Au-NC@UiO-68-NHC, and UiO-68-NH_2/Au mixture. (D) Time courses of CO evolution by PCR using UiO-68-NHC, Au-NC@UiO-68-NHC, UiO-68-NH_2, and Au/UiO-66-NH_2 as photocatalysts upon AM 1.5 G irradiation[107]. Copyright 2021 Wiley-VCH.

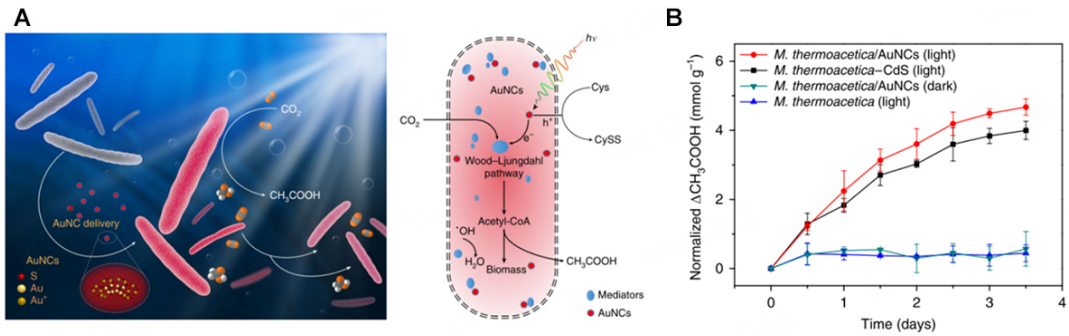

Figure 17. (A) Schematic diagram of the M. thermoacetica/Au NCs hybrid system. (B) photosynthesis behavior of different systems[109]. Copyright 2018, Springer Nature.

various advanced techniques have been widely explored. Due to the fast progress of this field, a summary of recent studies is essential for both new and experienced researchers in related fields. In this review, we summarize the recent advances in MNCs-based catalysts for PCR. We first introduce the synthesis of MNCs. Then, we explain the mechanism of photocatalysis based on MNCs-based catalysts. Finally, in the section on advanced MNCs-based catalysts for PCR, we classify MNCs into nonnoble MNCs and noble MNCs and summarize their role as catalysts in enhancing PCR performance. In the future, it is believed that there will be more strategies to optimize the design of MNCs-based catalysts for PCR. Therefore, we want to

emphasize the outlook for catalysts based on MNCs:

(1) The majority of current research is devoted to the development of transition MNCs. However, other types of NCs, such as alloy NCs, also merit investigation and consideration.

(2) The selectivity of CO_2 reduction by MNCs-based catalysts used to enhance the PCR process is still not good, and most systems can only reduce CO_2 to C_1 products such as CO. Therefore, how to improve the selectivity of PCR through material and system design is an important challenge at present.

(3) In the PCR process, MNCs are mostly used as co-catalysts/photosensitizers for semiconductor nanomaterials. It is hoped that in the future, there will be MNCs that can be used directly in PCR with excellent performance.

(4) The PCR efficiencies are still lower than commercial targets, and a firm understanding of how these rich structures of MNCs affect catalytic performance has yet to be fully achieved. The reaction pathways at the atomic level have yet to be determined. Therefore, further research should be dedicated to enhancing the activity of PCR processes and monitoring the structure of MNCs during reactions to further establish the precise correlation between structure and catalytic performance.

DECLARATIONS

Authors' contributions

Conceptualization, investigation, writing-original draft: Li H
Writing-review & editing: Luo H, Du H
Writing-review & editing, supervision, and funding acquisition: Wang H, Zhu W, Zhou Y

Availability of data and materials

Not applicable.

Financial support and sponsorship

This work was supported by the National Natural Science Foundation of China (22176086), the Natural Science Foundation of Jiangsu Province (BK20210189), State Key Laboratory of Pollution Control and Resource Reuse (PCRR-ZZ-202106), the Fundamental Research Funds for the Central Universities (021114380183, 021114380189, 021114380199), the Research Funds from the Nanjing Science and Technology Innovation Project for Chinese Scholars Studying Abroad (13006003), the Research Funds from Frontiers Science Center for Critical Earth Material Cycling of Nanjing University, and Research Funds for Jiangsu Distinguished Professor. Y.Z. would like to acknowledge the support from the National Natural Science Foundation of China (22276100), Natural Science Foundation of Jiangsu Province (SBK2022044384), Key Laboratory for Organic Electronics & Information Displays (GZR2022010010), Nanjing Science and Technology Innovation Project for Chinese Scholars Studying Abroad (NJKCZYZZ2022-01), Research Fund for Jiangsu Distinguished Professor (RK030STP22001), and the Research startup fund of NJUPT (NY221006).

Conflicts of interest

All authors declared that there are no conflicts of interest.

Ethical approval and consent to participate

Not applicable.

Consent for publication

Not applicable.

REFERENCES

1. Arneth A, Sitch S, Pongratz J, et al. Historical carbon dioxide emissions caused by land-use changes are possibly larger than assumed. *Nat Geosci* 2017;10:79-84. DOI
2. Liu LX, Fu J, Jiang LP, Zhang JR, Zhu W, Lin Y. Highly efficient photoelectrochemical reduction of CO_2 at low applied voltage using 3D Co-Pi/$BiVO_4$/SnO_2 nanosheet array photoanodes. *ACS Appl Mater Interfaces* 2019;11:26024-31. DOI
3. Yuan Y, Lu J. Demanding energy from carbon. *Carbon Energy* 2019;1:8-12. DOI
4. Liu J, Fu J, Zhou Y, Zhu W, Jiang LP, Lin Y. Controlled synthesis of EDTA-modified porous hollow copper microspheres for high-efficiency conversion of CO_2 to multicarbon products. *Nano Lett* 2020;20:4823-8. DOI
5. Liu J, Cai Y, Song R, et al. Recent progress on single-atom catalysts for CO_2 electroreduction. *Mater Today* 2021;48:95-114. DOI
6. Salemdeeb R, Saint R, Clark W, Lenaghan M, Pratt K, Millar F. A pragmatic and industry-oriented framework for data quality assessment of environmental footprint tools. *Resour Environ Sustain* 2021;3:100019. DOI
7. Dou X, Wang Y, Ciais P, et al. Near-real-time global gridded daily CO_2 emissions. *Innovation* 2022;3:100182. DOI PubMed PMC
8. Du H, Liu LX, Li P, et al. Enriching reaction intermediates in multishell structured copper catalysts for boosted propanol electrosynthesis from carbon monoxide. *ACS Nano* 2023;17:8663-70. DOI
9. Zhao Q, Yu P, Mahendran R, et al. Global climate change and human health: pathways and possible solutions. *Eco-Environ Health* 2022;1:53-62. DOI
10. Fu J, Li P, Lin Y, et al. Fight for carbon neutrality with state-of-the-art negative carbon emission technologies. *Eco-Environ Health* 2022;1:259-79. DOI
11. Li K, Cai Y, Yang X, et al. H_2S Involved photocatalytic system: a novel syngas production strategy by boosting the photoreduction of CO_2 while recovering hydrogen from the environmental toxicant. *Adv Funct Mater* 2022;32:2113002. DOI
12. Yang X, Li K, Wang G, et al. 2D Catalysts for CO_2 photoreduction: discussing structure efficiency strategies and prospects for scaled production based on current progress. *Chemistry* 2022;28:e202201881. DOI
13. Ran J, Jaroniec M, Qiao SZ. Cocatalysts in semiconductor-based photocatalytic CO_2 reduction: achievements, challenges, and opportunities. *Adv Mater* 2018;30:1704649. DOI PubMed
14. Fu J, Jiang K, Qiu X, Yu J, Liu M. Product selectivity of photocatalytic CO_2 reduction reactions. *Mater Today* 2020;32:222-43. DOI
15. Schäppi R, Rutz D, Dähler F, et al. Drop-in fuels from sunlight and air. *Nature* 2022;601:63-8. DOI
16. Tian J, Zhong K, Zhu X, et al. Highly exposed active sites of Au nanoclusters for photocatalytic CO_2 reduction. *Chem Eng J* 2023;451:138392. DOI
17. Yang J, Yang Z, Yang K, et al. Indium-based ternary metal sulfide for photocatalytic CO_2 reduction application. *Chin J Catal* 2023;44:67-95. DOI
18. Zhu L, Hu F, Sun B, Gu S, Gao T, Zhou G. Recent advances on multivariate MOFs for photocatalytic CO_2 reduction and H_2 evolution. *Adv Sustain Syst* 2023;7:2200394. DOI
19. Zhu Z, Xuan Y, Liu X, Zhu Q. Revealing the stochastic kinetics evolution of photocatalytic CO_2 reduction. *Nanoscale* 2023;15:730-41. DOI
20. Zuo Q, Cui R, Wang L, et al. High-loading single cobalt atoms on ultrathin MOF nanosheets for efficient photocatalytic CO_2 reduction. *Sci China Chem* 2023;66:570-7. DOI
21. Liu H, Zhu Y, Ma J, Zhang Z, Hu W. Recent advances in atomic-level engineering of nanostructured catalysts for electrochemical CO_2 reduction. *Adv Funct Mater* 2020;30:1910534. DOI
22. He L, Yuan J, Xia N, et al. Kernel tuning and nonuniform influence on optical and electrochemical gaps of bimetal nanoclusters. *J Am Chem Soc* 2018;140:3487-90. DOI
23. Bootharaju MS, Baek W, Lee S, Chang H, Kim J, Hyeon T. Magic-sized stoichiometric II-VI nanoclusters. *Small* 2021;17:e2002067. DOI
24. Busatto S, de Mello Donega C. Magic-size semiconductor nanostructures: where does the magic come from? *ACS Mater Au* 2022;2:237-49. DOI PubMed PMC
25. Wang Y, Zhou Y, Zhang Y, Buhro WE. Magic-size II-VI nanoclusters as synthons for flat colloidal nanocrystals. *Inorg Chem* 2015;54:1165-77. DOI
26. Kurashige W, Kumazawa R, Ishii D, et al. Au_{25}-loaded $BaLa_4Ti_4O_{15}$ water-splitting photocatalyst with enhanced activity and durability produced using new chromium oxide shell formation method. *J Phys Chem C* 2018;122:13669-81. DOI
27. Gautam A, Gore PM, Kandasubramanian B. Nanocluster materials in photosynthetic machines. *Chem Eng J* 2020;385:123951. DOI
28. Nitopi S, Bertheussen E, Scott SB, et al. Progress and perspectives of electrochemical CO_2 reduction on copper in aqueous electrolyte. *Chem Rev* 2019;119:7610-72. DOI

29. Shoji S, Yin G, Nishikawa M, Atarashi D, Sakai E, Miyauchi M. Photocatalytic reduction of CO_2 by CuO nanocluster loaded $SrTiO_3$ nanorod thin film. *Chem Phys Lett* 2016;658:309-14. DOI
30. Gao Y, Sun L, Bian J, Zhang Z, Li Z, Jing L. Accelerated charge transfer of g-C_3N_4/$BiVO_4$ Z-scheme 2D heterojunctions by controllably introducing phosphate bridges and Ag nanocluster co-catalysts for selective CO_2 photoreduction to CO. *Appl Surf Sci* 2023;610:155360. DOI
31. Bo Y, Du P, Li H, et al. Bridging Au nanoclusters with ultrathin LDH nanosheets via ligands for enhanced charge transfer in photocatalytic CO_2 reduction. *Appl Catal B Environ* 2023;330:122667. DOI
32. Chen J, Zhang QF, Bonaccorso TA, Williard PG, Wang LS. Controlling gold nanoclusters by diphospine ligands. *J Am Chem Soc* 2014;136:92-5. DOI
33. Zhu Q, Huang X, Zeng Y, et al. Controllable synthesis and electrocatalytic applications of atomically precise gold nanoclusters. *Nanoscale Adv* 2021;3:6330-41. DOI
34. Liu L, Corma A. Metal Catalysts for heterogeneous catalysis: from single atoms to nanoclusters and nanoparticles. *Chem Rev* 2018;118:4981-5079. DOI PubMed PMC
35. Chakraborty I, Pradeep T. Atomically precise clusters of noble metals: emerging link between atoms and nanoparticles. *Chem Rev* 2017;117:8208-71. DOI PubMed
36. Lu H, Chen B, Li Y, et al. Benzyl-rich ligand engineering of the photostability of atomically precise gold nanoclusters. *Chem Commun* 2022;58:2395-8. DOI
37. Fang J, Zhang B, Yao Q, Yang Y, Xie J, Yan N. Recent advances in the synthesis and catalytic applications of ligand-protected, atomically precise metal nanoclusters. *Coord Chem Rev* 2016;322:1-29. DOI
38. Chai OJH, Liu Z, Chen T, Xie J. Engineering ultrasmall metal nanoclusters for photocatalytic and electrocatalytic applications. *Nanoscale* 2019;11:20437-48. DOI
39. Sun Y, Cai X, Hu W, Liu X, Zhu Y. Electrocatalytic and photocatalytic applications of atomically precise gold-based nanoclusters. *Sci China Chem* 2021;64:1065-75. DOI
40. Wu J, Xia W, Lan M, et al. Artificial photosynthetic assemblies constructed by the self-assembly of synthetic building blocks for enhanced photocatalytic hydrogen evolution. *J Mater Chem A* 2020;8:21690-9. DOI
41. Yao Q, Chen T, Yuan X, Xie J. Toward total synthesis of thiolate-protected metal nanoclusters. *ACC Chem Res* 2018;51:1338-48. DOI
42. Luo Z, Nachammai V, Zhang B, et al. Toward understanding the growth mechanism: tracing all stable intermediate species from reduction of Au(I)-thiolate complexes to evolution of Au_{25} nanoclusters. *J Am Chem Soc* 2014;136:10577-80. DOI
43. Yao Q, Yuan X, Fung V, et al. Understanding seed-mediated growth of gold nanoclusters at molecular level. *Nat Commun* 2017;8:927. DOI PubMed PMC
44. Wang S, Li Q, Kang X, Zhu M. Customizing the structure, composition, and properties of alloy nanoclusters by metal exchange. *ACC Chem Res* 2018;51:2784-92. DOI
45. Li Y, Zhou M, Jin R. Programmable metal nanoclusters with atomic precision. *Adv Mater* 2021;33:e2006591. DOI
46. Li G, Jin R. Atomically precise gold nanoclusters as new model catalysts. *ACC Chem Res* 2013;46:1749-58. DOI
47. Zhou M, Higaki T, Li Y, et al. Three-stage evolution from nonscalable to scalable optical properties of thiolate-protected gold nanoclusters. *J Am Chem Soc* 2019;141:19754-64. DOI
48. Pan H, Heagy MD. Photons to formate-a review on photocatalytic reduction of CO_2 to formic acid. *Nanomaterials* 2020;10:2422. DOI PubMed PMC
49. Linsebigler AL, Lu G, Yates JT. Photocatalysis on TiO_2 surfaces: principles, mechanisms, and selected results. *Chem Rev* 1995;95:735-58. DOI
50. Habisreutinger SN, Schmidt-mende L, Stolarczyk JK. Photokatalytische reduktion von CO_2 an TiO_2 und anderen halbleitern. *Angew Chem Int Ed* 2013;125:7516-57. DOI
51. Yan J, Teo BK, Zheng N. Surface chemistry of atomically precise coinage-metal nanoclusters: from structural control to surface reactivity and catalysis. *ACC Chem Res* 2018;51:3084-93. DOI PubMed
52. Hou B, Kim B, Lee HKH, et al. Multiphoton absorption stimulated metal chalcogenide quantum dot solar cells under ambient and concentrated irradiance. *Adv Funct Mater* 2020;30:2004563. DOI
53. Guo K, Zhu X, Peng L, et al. Boosting photocatalytic CO_2 reduction over a covalent organic framework decorated with ruthenium nanoparticles. *Chem Eng J* 2021;405:127011. DOI
54. Kuhl KP, Cave ER, Abram DN, Jaramillo TF. New insights into the electrochemical reduction of carbon dioxide on metallic copper surfaces. *Energy Environ Sci* 2012;5:7050. DOI
55. Zhou M, Wang S, Yang P, Huang C, Wang X. Boron carbon nitride semiconductors decorated with CdS nanoparticles for photocatalytic reduction of CO_2. *ACS Catal* 2018;8:4928-36. DOI
56. Nguyen D, Nguyen C, Do T. Rational one-step synthesis of cobalt clusters embedded-graphitic carbon nitrides for the efficient photocatalytic CO_2 reduction under ambient conditions. *J Catal* 2020;392:88-96. DOI
57. Hansen HA, Varley JB, Peterson AA, Nørskov JK. Understanding trends in the electrocatalytic activity of metals and enzymes for CO_2 reduction to CO. *J Phys Chem Lett* 2013;4:388-92. DOI
58. Rosen BA, Salehi-Khojin A, Thorson MR, et al. Ionic liquid-mediated selective conversion of CO_2 to CO at low overpotentials. *Science* 2011;334:643-4. DOI

59. Palencia C, Yu K, Boldt K. The future of colloidal semiconductor magic-size clusters. *ACS Nano* 2020;14:1227-35. DOI PubMed
60. Chang X, Wang T, Gong J. CO_2 photo-reduction: insights into CO_2 activation and reaction on surfaces of photocatalysts. *Energy Environ Sci* 2016;9:2177-96. DOI
61. Peng S, Zeng X, Li Y. Titanate nanotube modified with different nickel precursors for enhanced Eosin Y-sensitized photocatalytic hydrogen evolution. *Int J Hydrog Energy* 2015;40:6038-49. DOI
62. Zhang W, Li Y, Zeng X, Peng S. Synergetic effect of metal nickel and graphene as a cocatalyst for enhanced photocatalytic hydrogen evolution via dye sensitization. *Sci Rep* 2015;5:10589. DOI PubMed PMC
63. Li Y, Xiang Y, Peng S, Wang X, Zhou L. Modification of Zr-doped titania nanotube arrays by urea pyrolysis for enhanced visible-light photoelectrochemical H_2 generation. *Electrochim Acta* 2013;87:794-800. DOI
64. Yin G, Nishikawa M, Nosaka Y, et al. Photocatalytic carbon dioxide reduction by copper oxide nanocluster-grafted niobate nanosheets. *ACS Nano* 2015;9:2111-9. DOI
65. Park D, Jeong Y, Lee J, Lee J, Moon S. Interfacial charge-transfer loss in dye-sensitized solar cells. *J Phys Chem C* 2013;117:2734-9. DOI
66. Irie H, Miura S, Kamiya K, Hashimoto K. Efficient visible light-sensitive photocatalysts: Grafting Cu(II) ions onto TiO_2 and WO_3 photocatalysts. *Chem Phys Lett* 2008;457:202-5. DOI
67. Irie H, Kamiya K, Shibanuma T, et al. Visible light-sensitive Cu(II)-grafted TiO_2 photocatalysts: activities and X-ray absorption fine structure analyses. *J Phys Chem C* 2009;113:10761-6. DOI
68. Yu H, Irie H, Shimodaira Y, et al. An efficient visible-light-sensitive Fe(III)-grafted TiO_2 photocatalyst. *J Phys Chem C* 2010;114:16481-7. DOI
69. Liu M, Qiu X, Hashimoto K, Miyauchi M. Cu(II) nanocluster-grafted, Nb-doped TiO_2 as an efficient visible-light-sensitive photocatalyst based on energy-level matching between surface and bulk states. *J Mater Chem A* 2014;2:13571-9. DOI
70. Miyauchi M, Irie H, Liu M, et al. Visible-light-sensitive photocatalysts: nanocluster-grafted titanium dioxide for indoor environmental remediation. *J Phys Chem Lett* 2016;7:75-84. DOI
71. Kong L, Wang C, Wan F, Zheng H, Zhang X. Synergistic effect of surface self-doping and Fe species-grafting for enhanced photocatalytic activity of TiO_2 under visible-light. *Appl Surf Sci* 2017;396:26-35. DOI
72. Ji Y, Luo Y. New Mechanism for photocatalytic reduction of CO_2 on the anatase TiO_2 (101) surface: the essential role of oxygen vacancy. *J Am Chem Soc* 2016;138:15896-902. DOI PubMed
73. Nolan M, Iwaszuk A, Gray KA. Localization of photoexcited electrons and holes on low coordinated Ti and O sites in free and supported TiO_2 nanoclusters. *J Phys Chem C* 2014;118:27890-900. DOI
74. Hurum D, Agrios A, Crist S, Gray K, Rajh T, Thurnauer M. Probing reaction mechanisms in mixed phase TiO_2 by EPR. *J Electron Spectros Relat Phenomena* 2006;150:155-63. DOI
75. Li G, Gray KA. The solid-solid interface: explaining the high and unique photocatalytic reactivity of TiO_2-based nanocomposite materials. *Chem Phys* 2007;339:173-87. DOI
76. Pacchioni G. Oxygen vacancy: the invisible agent on oxide surfaces. *Chemphyschem* 2003;4:1041-7. DOI PubMed
77. Liu M, Qiu X, Miyauchi M, Hashimoto K. Energy-level matching of Fe(III) ions grafted at surface and doped in bulk for efficient visible-light photocatalysts. *J Am Chem Soc* 2013;135:10064-72. DOI PubMed
78. Liu M, Sunada K, Hashimoto K, Miyauchi M. Visible-light sensitive Cu(II)-TiO_2 with sustained anti-viral activity for efficient indoor environmental remediation. *J Mater Chem A* 2015;3:17312-9. DOI
79. Liu M, Inde R, Nishikawa M, et al. Enhanced photoactivity with nanocluster-grafted titanium dioxide photocatalysts. *ACS Nano* 2014;8:7229-38. DOI
80. Cheng L, Li B, Yin H, Fan J, Xiang Q. Cu clusters immobilized on Cd-defective cadmium sulfide nano-rods towards photocatalytic CO_2 reduction. *J Mater Sci Technol* 2022;118:54-63. DOI
81. Billo T, Fu FY, Raghunath P, et al. Ni-nanocluster modified black TiO_2 with dual active sites for selective photocatalytic CO_2 reduction. *Small* 2018;14:1702928. DOI
82. Li Y, Wang C, Song M, Li D, Zhang X, Liu Y. TiO_{2-x}/CoO_x photocatalyst sparkles in photothermocatalytic reduction of CO_2 with H_2O steam. *Appl Catal B Environ* 2019;243:760-70. DOI
83. Hou T, Luo N, Cui Y, et al. Selective reduction of CO_2 to CO under visible light by controlling coordination structures of CeO_x-S/$ZnIn_2S_4$ hybrid catalysts. *Appl Catal B Environ* 2019;245:262-70. DOI
84. Mrowetz M, Villa A, Prati L, Selli E. Effects of Au nanoparticles on TiO_2 in the photocatalytic degradation of an azo dye. *Gold Bull* 2007;40:154-60. DOI
85. Yadav A, Li Y, Liao TW, et al. Enhanced methanol electro-oxidation activity of nanoclustered gold. *Small* 2021;17:e2004541. DOI
86. Liao TW, Verbruggen SW, Claes N, et al. TiO_2 films modified with Au nanoclusters as self-cleaning surfaces under visible light. *Nanomaterials* 2018;8:30. DOI PubMed PMC
87. Li Y, Yang Y, Chen G, Fan J, Xiang Q. Au cluster anchored on TiO_2/Ti_3C_2 hybrid composites for efficient photocatalytic CO_2 reduction. *Rare Met* 2022;41:3045-59. DOI
88. Xiao FX, Zeng Z, Hsu SH, Hung SF, Chen HM, Liu B. Light-induced *in situ* transformation of metal clusters to metal nanocrystals for photocatalysis. *ACS Appl Mater Interfaces* 2015;7:28105-9. DOI PubMed
89. Liu S, Xu YJ. Photo-induced transformation process at gold clusters-semiconductor interface: implications for the complexity of gold clusters-based photocatalysis. *Sci Rep* 2016;6:22742. DOI

90. Zhou P, Yu J, Jaroniec M. All-solid-state Z-scheme photocatalytic systems. *Adv Mater* 2014;26:4920-35. DOI
91. Bard AJ. Photoelectrochemistry and heterogeneous photo-catalysis at semiconductors. *J Photochem* 1979;10:59-75. DOI
92. Li H, Tu W, Zhou Y, Zou Z. Z-scheme photocatalytic systems for promoting photocatalytic performance: recent progress and future challenges. *Adv Sci* 2016;3:1500389. DOI PubMed PMC
93. Maeda K. Z-scheme water splitting using two different semiconductor photocatalysts. *ACS Catal* 2013;3:1486-503. DOI
94. Xu Q, Zhang L, Cheng B, Fan J, Yu J. S-scheme heterojunction photocatalyst. *Chem* 2020;6:1543-59. DOI
95. Deng Y, Zhang Z, Du P, et al. Embedding ultrasmall Au clusters into the pores of a covalent organic framework for enhanced photostability and photocatalytic performance. *Angew Chem Int Ed* 2020;132:6138-45. DOI
96. Xu Q, Wageh S, Al-ghamdi AA, Li X. Design principle of S-scheme heterojunction photocatalyst. *J Mater Sci Technol* 2022;124:171-3. DOI
97. Li X, Xiong J, Gao X, et al. Novel BP/BiOBr S-scheme nano-heterojunction for enhanced visible-light photocatalytic tetracycline removal and oxygen evolution activity. *J Hazard Mater* 2020;387:121690. DOI
98. Xia P, Cao S, Zhu B, et al. Designing a 0D/2D S-scheme heterojunction over polymeric carbon nitride for visible-light photocatalytic inactivation of bacteria. *Angew Chem Int Ed* 2020;59:5218-25. DOI
99. Xu F, Meng K, Cheng B, Wang S, Xu J, Yu J. Unique S-scheme heterojunctions in self-assembled TiO_2/$CsPbBr_3$ hybrids for CO_2 photoreduction. *Nat Commun* 2020;11:4613. DOI PubMed PMC
100. Wageh S, A. Al-ghamdi A, Liu L. S-scheme heterojunction photocatalyst for CO_2 photoreduction. *Acta Physico-Chimica Sinica* 2021;37:2010024. DOI
101. Zhang L, Zhang J, Yu H, Yu J. Emerging S-scheme photocatalyst. *Adv Mater* 2022;34:e2107668. DOI
102. Ke X, Zhang J, Dai K, Fan K, Liang C. Integrated S-scheme heterojunction of amine-functionalized 1D CdSe nanorods anchoring on ultrathin 2D $SnNb_2O_6$ Nanosheets for robust solar-driven CO_2 conversion. *Solar RRL* 2021;5:2000805. DOI
103. Férey G. Hybrid porous solids: past, present, future. *Chem Soc Rev* 2008;37:191-214. DOI PubMed
104. Long JR, Yaghi OM. The pervasive chemistry of metal-organic frameworks. *Chem Soc Rev* 2009;38:1213-4. DOI PubMed
105. Bernales V, Ortuño MA, Truhlar DG, Cramer CJ, Gagliardi L. Computational design of functionalized metal-organic framework nodes for catalysis. *ACS Cent Sci* 2018;4:5-19. DOI PubMed PMC
106. Choudhuri I, Truhlar DG. Photogenerated charge separation in a CdSe nanocluster encapsulated in a metal-organic framework for improved photocatalysis. *J Phys Chem C* 2020;124:8504-13. DOI
107. Jiang Y, Yu Y, Zhang X, et al. N-heterocyclic carbene-stabilized ultrasmall gold nanoclusters in a metal-organic framework for photocatalytic CO_2 reduction. *Angew Chem Int Ed* 2021;60:17388-93. DOI
108. Sakimoto KK, Kornienko N, Yang P. Cyborgian material design for solar fuel production: the emerging photosynthetic biohybrid systems. *ACC Chem Res* 2017;50:476-81. DOI PubMed
109. Zhang H, Liu H, Tian Z, et al. Bacteria photosensitized by intracellular gold nanoclusters for solar fuel production. *Nat Nanotechnol* 2018;13:900-5. DOI